sustainability

MDPI

Article

Facile Recovery of Polycationic Metals from Acid Mine Drainage and Their Subsequent Valorisation for the Treatment of Municipal Wastewater

Khathutshelo Lilith Muedi [1], Job Tatenda Tendenedzai [1], Vhahangwele Masindi [2], Nils Hendrik Haneklaus [3,4,*] and Hendrik Gideon Brink [1,*]

[1] Department of Chemical Engineering, Faculty of Engineering, Built Environment and Information Technology, University of Pretoria, Private Bag X20, Hatfield 0028, South Africa; khathumuedi@gmail.com (K.L.M.); job.tendenedzai@tuks.co.za (J.T.T.)
[2] Department of Environmental Sciences, School of Agriculture and Environmental Sciences, University of South Africa (UNISA), P.O. Box 392, Florida 1710, South Africa; emasinv@unisa.ac.za
[3] Td-Lab Sustainable Mineral Resources, University for Continuing Education Krems, Dr.-Karl-Dorrek-Straße 30, 3500 Krems, Austria
[4] Unit for Energy and Technology Systems—Nuclear Engineering, North-West University, 11 Hoffman Street, Potchefstroom 2520, South Africa
* Correspondence: nils.haneklaus@donau-uni.ac.at (N.H.H.); deon.brink@up.ac.za (H.G.B.)

Abstract: The presence of toxic and hazardous chemical species in municipal wastewater poses a significant environmental and public health challenge, necessitating innovative, sustainable, and cost-effective treatment solutions. This study pioneers the recovery and valorisation of polycationic metals from real acid mine drainage (AMD) for municipal wastewater treatment, demonstrating a novel approach that integrates resource recovery with wastewater remediation. A key strength of this study is the use of real municipal wastewater (authentic MWW) in the treatment phase, ensuring that the findings accurately reflect real-world conditions. Advanced analytical techniques were employed to characterise both aqueous and solid samples, and batch experiments were conducted to assess the removal efficiency of polycationic metals for key contaminants: ammonium (NH_4^+), sulphate (SO_4^{2-}), phosphate (PO_4^{3-}), and nitrate (NO_3^-). The optimised conditions are 2 g of polycationic metals per 100 mL, 90 min of contact time, and 35 °C. The yielded exceptional removal efficiencies are PO_4^{3-} (>99.9%), NH_4^+ (>99.7%), NO_3^- (>99%), and SO_4^{2-} (>96%), achieving final concentrations of <0.5 mg/L for PO_4^{3-} and NH_4^+, 2.1 mg/L for NO_3^-, and 9.1 mg/L for SO_4^{2-}. Adsorption kinetics followed a pseudo-first-order model, indicating physisorption, while the Two-Surface Langmuir model suggested a combination of homogeneous and heterogeneous adsorption mechanisms. FTIR, SEM-EDX mapping, and XRF analyses confirmed the retention of P, S, and N in the product sludge, validating the adsorption process. This study is the first of its kind to recover Al-rich Fe species from real AMD and activate them for municipal wastewater remediation using authentic MWW, bridging the gap between laboratory-scale research and real-world applications. By simultaneously addressing AMD pollution and municipal wastewater treatment, this research advances circular economy principles, promotes sustainable water management, and contributes to national and global efforts toward water security and environmental protection.

Keywords: resource recovery; environmental remediation; sustainable wastewater treatment; industrial effluent management; nutrient sequestration; waste valorisation; circular economy in water treatment

Academic Editor: Agostina Chiavola

Received: 4 February 2025
Revised: 11 March 2025
Accepted: 14 March 2025
Published: 18 March 2025

Citation: Muedi, K.L.; Tendenedzai, J.T.; Masindi, V.; Haneklaus, N.H.; Brink, H.G. Facile Recovery of Polycationic Metals from Acid Mine Drainage and Their Subsequent Valorisation for the Treatment of Municipal Wastewater. *Sustainability* **2025**, *17*, 2701. https://doi.org/10.3390/su17062701

1. Introduction

Water pollution is a critical environmental issue with direct implications for several United Nations Sustainable Development Goals (SDGs). It poses significant public health risks by contaminating water sources with harmful pathogens and chemicals, which directly threatens SDG 3: Good Health and Well-Being, by increasing the spread of waterborne diseases and contributing to health crises [1]. The pollution of freshwater resources also impedes progress toward SDG 6: Clean Water and Sanitation, as contaminated water increases the need for more complex and costly treatment processes to ensure safe water access [2]. Economically, water pollution imposes substantial financial burdens due to the increased costs of water treatment and purification processes required to make water safe for consumption and use (SDG 12: Responsible Consumption and Production) [3]. Additionally, water pollution disrupts aquatic ecosystems, causing biodiversity loss and degrading natural habitats, which impacts SDG 14: Life Below Water, by harming marine and freshwater species and reducing the sustainability of aquatic environments [4]. Sustainable practices for water pollution control are essential for achieving these interconnected goals, ensuring the well-being of human populations and the preservation of ecosystems.

In recent years, acid mine drainage (AMD) has emerged as a significant environmental challenge due to its high acidity and elevated concentrations of dissolved heavy metals, such as iron (Fe), aluminium (Al), zinc (Zn), copper (Cu), manganese (Mn), and cadmium (Cd) [5]. Acid mine drainage is generated when sulphide minerals, commonly found in mine waste, are exposed to air and water, leading to a series of oxidation reactions [6]. The sulphide oxidation reaction of pyrite (FeS_2) in the presence of water is shown in Equation (1). This reaction produces ferrous iron (Fe^{2+}), sulphate ions ($SO_4{}^{2-}$), and hydrogen ions (H^+), which contribute to the high acidity of AMD.

$$2FeS_{2(s)} + 7O_{2(g)} + 2H_2O_{(l)} \rightarrow 2Fe^{2+}_{(aq)} + 4SO^{2-}_{4(aq)} + 4H^+_{(aq)} \quad (1)$$

The ferrous iron can further oxidise to ferric iron (Fe^{3+}), which precipitates as iron hydroxide, creating even more acidity, as illustrated in Equations (2) and (3).

$$Fe^{2+}_{(aq)} + \frac{1}{4}O_{2(g)} + H^+_{(aq)} \rightarrow Fe^{3+}_{(aq)} + \frac{1}{2}H_2O_{(l)} \quad (2)$$

$$Fe^{3+}_{(aq)} + 3H_2O_{(l)} \rightarrow Fe(OH)_{3(s)} + 3H^+_{(aq)} \quad (3)$$

The high acidity and metal concentrations in AMD pose severe threats to aquatic ecosystems and water quality. The low pH of AMD can lead to the dissolution of toxic metals, such as aluminium, manganese, and other heavy metals, which can harm aquatic life and contaminate drinking water sources [7]. Equation (4) illustrates the dissolution of aluminium as one of the heavy metals in the AMD.

$$Al(OH)_{3(s)} + 3H^+_{(aq)} \rightarrow Al^{3+}_{(aq)} + 3H_2O_{(l)} \quad (4)$$

The treatment of acid mine drainage (AMD) involves a variety of technologies, including adsorption, which uses high-surface-area materials to selectively capture metals from AMD [8]. Membrane filtration technologies, such as microfiltration, ultrafiltration, nanofiltration, and reverse osmosis, are also commonly employed to separate dissolved metals from AMD using semi-permeable membranes [9]. Another effective approach is ion exchange, where ion exchange resins selectively remove metal ions from AMD through functional group interactions [10]. Additionally, bioremediation uses biological agents, such as bacteria and algae, to bioaccumulate or precipitate metals. Anekwe et al. [11] conducted a review on the bioremediation of AMD, highlighting the use of biological

agents like bacteria and algae to facilitate the bioaccumulation or precipitation of metals through metabolic processes.

Beyond these treatment methods, the recovery and utilisation of heavy metals and minerals from AMD have gained significant interest due to the abundance of valuable metals like iron and aluminium. These metals, found in high concentrations in AMD, are ideal candidates for recovery and valorisation, particularly for environmental remediation and wastewater treatment applications [6,12]. AMD-recovered minerals have shown great potential in these fields due to their unique physicochemical properties, including a high surface area, enhanced reactivity, and superior adsorption capacity [13,14]. These properties make them particularly effective in removing contaminants from wastewater through adsorption, as the high surface area of the nanocomposites allows for greater interaction with pollutants, while their enhanced reactivity ensures efficient contaminant removal [15,16]. The recovery of minerals from AMD involves a range of advanced technologies aimed at reclaiming valuable metals and mitigating environmental impacts. One common method is precipitation, where chemical reagents are added to AMD to form insoluble metal compounds that are then separated [17–19]. This method is effective in recovering metals such as Fe, Al, and Mn by adjusting the pH of AMD to induce the formation of metal hydroxides [20,21]. Building on the previous work of our research group [22–24], this study explores the recovery of Fe and Al species from AMD and evaluates their application for the removal of contaminants from real municipal wastewater (authentic MWW). By combining recovery and remediation strategies, this approach offers a sustainable solution to AMD pollution.

Among the various sources of water pollution, authentic MWW is a significant contributor, often containing harmful contaminants such as ammonium (NH_4^+), sulphate (SO_4^{2-}), phosphate (PO_4^{3-}), and nitrate (NO_3^-) [25]. These pollutants stem from domestic activities, industrial processes, and agricultural runoff, posing serious risks to both human health and the environment [26]. Akinnawo et al. [27] highlighted that NH_4^+ is toxic to aquatic organisms, while high levels of SO_4^{2-}, PO_4^{3-}, and NO_3^-, can lead to eutrophication, causing algal blooms and oxygen depletion in water bodies. Consequently, the effective treatment of authentic MWW is crucial to ensure compliance with acceptable water standards and to prevent adverse ecological impacts [28].

Traditional methods for removing NH_4^+, SO_4^{2-}, PO_4^{3-}, and NO_3^-, such as chemical precipitation, ion exchange, and biological treatment, often face limitations in terms of efficiency and cost [29–31]. This has led to a growing demand for innovative and sustainable alternatives that not only improve the efficiency of contaminant removal but also offer cost-effective and environmentally friendly solutions. One promising approach is the use of advanced nanostructured materials, such as polycationic metals, which demonstrate superior performance in the removal of pollutants from wastewater through adsorption.

This study explores the feasibility and efficacy of polycationic metals recovered from real AMD for the removal of SO_4^{2-}, NH_4^+, PO_4^{3-}, and NO_3^- from authentic MWW through adsorption. To the best of the authors' knowledge, this is the first study to investigate the recovery of polycationic species from authentic AMD and their application for the effective removal of contaminants from authentic MWW. The findings of this research offer significant environmental benefits, advancing circular economy principles by promoting waste valorisation and beneficiation while simultaneously minimising ecological footprints. Unlike conventional approaches that focus solely on AMD neutralisation and secondary sludge disposal, this study demonstrates a resource-recovery-driven approach that repurposes AMD-derived materials for pollutant removal. The accumulation of secondary sludge from hazardous AMD has been widely recognized as a major environmental and

economic burden [13], increasing remediation costs for mining operations and posing risks to human and ecological health.

By recovering valuable minerals from real AMD and synthesising a polycationic adsorbent for wastewater treatment, this study introduces a sustainable and cost-effective solution that addresses both AMD pollution and municipal wastewater contamination, offering a dual environmental benefit.

2. Materials and Methods

2.1. Feedstock Collection and Sample Preparation

Raw acid mine drainage (AMD) was sourced from industrial coal mining activities in the Mpumalanga Province, South Africa, while authentic MWW was collected from a wastewater treatment plant in Gauteng Province. Chemical reagents including ammonium chloride (NH_4Cl), disodium phosphate (Na_2HPO_4), sodium nitrate ($NaNO_3$), caustic soda (NaOH), magnesium sulphate heptahydrate ($MgSO_4{\cdot}7H_2O$), and hydrochloric acid (37% HCl) were procured from Sigma-Aldrich and used without further purification. Ultra-pure water (18.2 MΩ cm resistivity) generated by the Elga PURELAB® Flex system was used for all aqueous solutions. The prepared solutions were comprised of 420 mg/L, 180 mg/L, 226 mg/L, and 253 mg/L for phosphate, ammonia, nitrate, and sulphate, respectively, to correspond to the measured values in the authentic MWW. All glassware was meticulously cleaned before and after each use to prevent cross-contamination.

2.2. Synthesis of Polycationic Metals

Polycationic metals were synthesised following an established procedure [22]. Acid mine drainage was diluted with NaOH to adjust the pH to 4.5, followed by agitation for 60 min at room temperature. The solution was then heated to 100 °C with continuous stirring, after which the precipitate was collected via vacuum filtration, dried, and ground into fine powder using a vibrating ball mill. The material was further calcined at 750 °C and sieved to a particle size of 32 µm. The final product was stored in airtight bags to avoid contamination.

2.3. Preparation of Synthetic Wastewater

Synthetic wastewater stock solutions were prepared by dissolving NH_4Cl, Na_2HPO_4, $MgSO_4{\cdot}7H_2O$, and $NaNO_3$ in 1 L of ultra-pure water. Fresh solutions were made from this stock for each batch experiment to optimise removal parameters.

2.4. Obtaining and Preparation of Authentic MWW Samples

Authentic MWW was sourced from the inlet of the activated sludge treatment process at an operational authentic MWW plant in Tshwane, South Africa (coordinates: 25°44′01.9″ S, 28°10′40.4″ E). The plant layout and operations are detailed by Muloiwa et al. [32]. To achieve the required nutrient concentrations for the isotherm experiments, the authentic MWW was spiked with varying amounts of NH_4Cl, Na_2HPO_4, $MgSO_4{\cdot}7H_2O$, and $NaNO_3$.

2.5. Batch Adsorption Experiments

Two separate batch adsorption experiments were performed to assess the removal of SO_4^{2-}, NH_4^+, PO_4^{3-}, and NO_3^- using the synthesised polycationic metals. In the first experiment, synthetic wastewater was used to reduce potential confounding factors, and the variables such as adsorbent dosage (ranging from 0.1 to 2 g), agitation time (10 to 300 min), operational temperature (25 to 55 °C), and pH (5 to 10) were optimised. All reactions were carried out at 300 rpm in 100 mL vessels.

The second experiment used authentic MWW, with unspiked authentic MWW for kinetic studies and spiked authentic MWW for isotherm analysis. This provided a more realistic evaluation of the adsorbent's performance in a real wastewater setting.

All results were obtained in triplicate and are reported as mean values.

2.6. Sample Characterisation

Aqueous samples were characterised for concentrations of SO_4^{2-}, NH_4^+, PO_4^{3-}, and NO_3^- using Ion Chromatography Mass Spectrometry (IC-MS: 940 Professional IC Vario). The pH of the solutions was measured using a Thermo Scientific™ Orion 3 Star portable pH meter, and electrical conductivity (EC), total dissolved solids (TDSs), and salinity were measured using a Mettler Toledo FiveGo EC/TDS/Salt/Temperature portable multimeter.

2.7. Sludge Characterisation

Solid samples were analysed before and after the authentic MWW adsorption experiments (experiment 2) using Fourier Transform Infrared Spectroscopy (FTIR—Bruker FTIR Spectrometer Alpha II Platinum-ATR with OPUS Version 8.2 TOUCH IR Spectroscopy Software, Bruker BioSpin AG, Fällanden, Switzerland), High-Resolution Scanning Electron Microscopy with Energy Dispersive X-Ray Spectroscopy (HR-SEM-EDX) (Carl Zeiss Sigma VP FE-SEM with Oxford EDX Sputtering System, Carl Zeiss AG, Oberkochen, Germany), and X-Ray Fluorescence (XRF) (Thermo Fisher ARL Perform'X Sequential XRF instrument with Uniquant Sulphide software, Thermo Fisher Scientific, Waltham, MA, USA) to evaluate functional groups, surface morphology, and elemental composition, respectively.

The HR-SEM-EDX elemental mapping was utilised to analyse the correlation between elements on the adsorbent surface, following the approach initially presented by Kpai et al. [33]. In brief, EDS maps for different elements were quantitatively compared by standardising image dimensions and pixel alignment using the Python Image Library (PIL Version 1.1). The images were cropped to uniform sizes and coordinates, converted to grayscale, and transformed into numerical matrices representing pixel luminescence values, which correspond to relative elemental concentrations. These matrices were then flattened and analysed using Pearson's correlation coefficient (numpy corrcoef) to evaluate elemental distribution patterns and potential interactions or bonding relationships across the adsorbent surface.

3. Results and Discussion

3.1. Water Quality Results

This section outlines the process to determine the optimised conditions under which the contaminants NH_4^+, SO_4^{2-}, PO_4^{3-}, and NO_3^- can be most effectively removed from authentic MWW. The results for the dosage, contact time, and temperature variations are reported in Figure 1.

3.1.1. Effect of Dosage

The attenuation of contaminants from authentic MWW as a function of dosage is shown in Figure 1a. The relationship between the residual concentrations of SO_4^{2-}, NH_4^+, PO_4^{3-}, and NO_3^- and polycationic metal dosage is presented. The polycationic metals showed high potential for removing SO_4^{2-} from the wastewater, achieving a removal efficiency of ≥90%. For PO_4^{3-}, the highest removal (≥90%) was observed at an adsorbent concentration of 2 g/100 mL. However, some resistance to removal was noted between 0.2 and 1 g/100 mL, which was overcome at higher dosages of 1.5–2 g/100 mL. NO_3^- removal was ≥90% at a dosage of 0.5 g/100 mL, while NH_4^+ was completely removed (≥99.99%) at a dosage of 1 g/100 mL. The increase in dosage resulted in higher removal efficiencies,

indicating that more surface area was available for the adsorption process. Based on these results, a dosage of 1.5 g/100 mL was identified as the optimum condition for the removal of contaminants from wastewater using polycationic metals recovered from acid mine drainage.

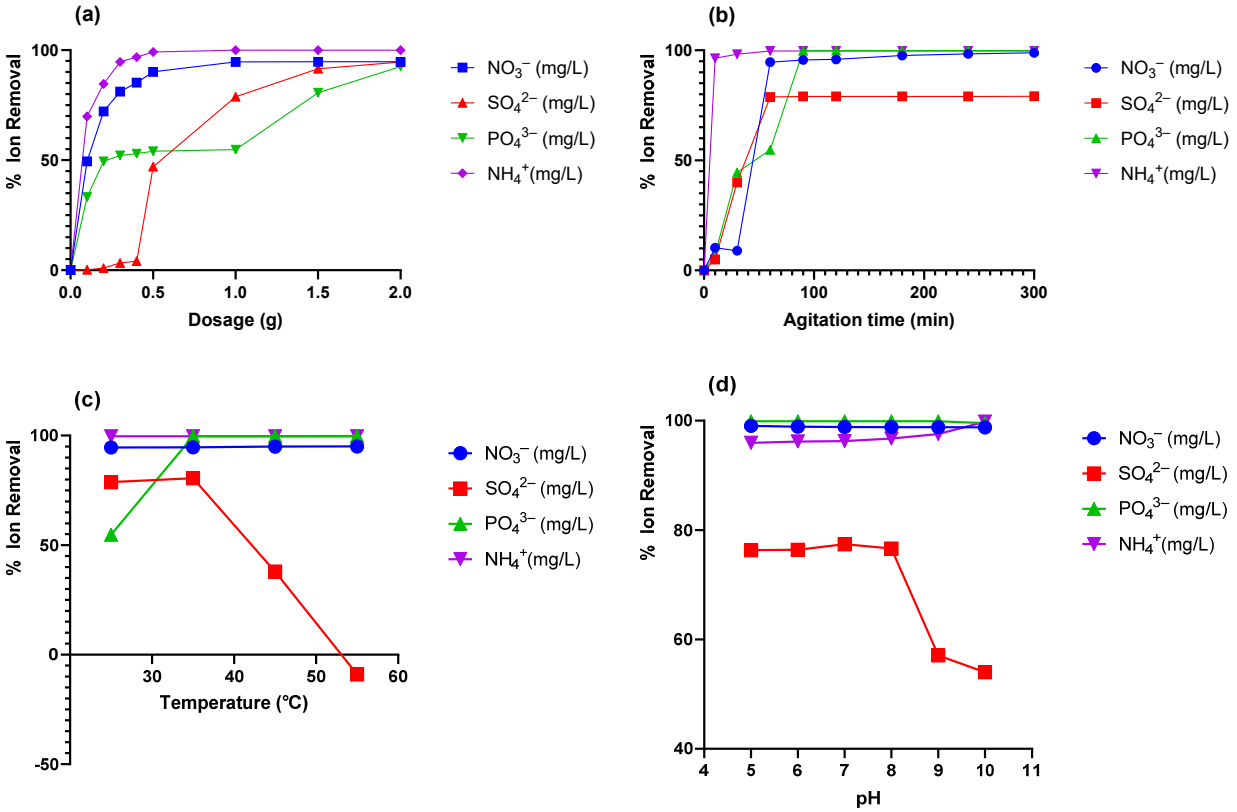

Figure 1. Attenuation of contaminants from synthetic municipal wastewater as a function of (**a**) dosage (conditions: 100 mL synthetic municipal wastewater, ambient temperature, neutral pH, and passive mixing for 60 min), (**b**) contact time (conditions: 100 mL synthetic municipal wastewater, ambient temperature, neutral pH, and feed dosage of 1 g), (**c**) temperature (conditions: 100 mL synthetic municipal wastewater, passive mixing for 60 min, neutral pH, and feed dosage of 1 g), and (**d**) pH (conditions: 100 mL synthetic municipal wastewater, passive mixing for 60 min, ambient temperature, and feed dosage of 1 g).

These findings are consistent with previous studies. For instance, Cheng et al. [34] reported 90% removal of NO_3^- from wastewater using 50 mg/L of Fe-Al bimetal. Similarly, Xu et al. [35] achieved 90% removal of PO_4^{3-} using 18.25 mg/L of $FeSO_4$-$Al_2(SO_4)_3$ coagulant. Additionally, Nurmesniemi et al. [36] demonstrated that SO_4^{2-} can be removed from wastewater with 87% efficiency using calcium sulfoaluminate ($Ca_4Al_6O_{12}SO_4$).

3.1.2. Effect of Contact Time

The attenuation of contaminants from synthetic municipal wastewater as a function of contact time is shown in Figure 1b. This figure illustrates the relationship between the residual concentrations of SO_4^{2-}, NH_4^+, PO_4^{3-}, and NO_3^- and the agitation time. The polycationic metals demonstrated the ability to remove approximately 80% of SO_4^{2-} from the aqueous solution after 60 min of equilibration. For NO_3^-, a removal efficiency of ≥99% was achieved after 90 min. PO_4^{3-} was almost completely removed (≥99.99%) at 90 min, while NH_4^+ was fully removed by the 60 min mark. Based on these findings, 90 min was determined to be the optimum equilibration time for the removal of SO_4^{2-}, NH_4^+, PO_4^{3-}, and NO_3^- from the wastewater system.

These results align with previous studies, such as Cheng et al. [34], who reported a 90% removal of NO_3^- from wastewater using Fe-Al bimetal, with an optimal contact time of 60 min.

3.1.3. Effect of Temperature

The attenuation of contaminants from synthetic municipal wastewater as a function of temperature is summarised in Figure 1c. This figure highlights the relationship between the residual concentrations of SO_4^{2-}, NH_4^+, PO_4^{3-}, and NO_3^- at different temperatures. Polycationic metals demonstrated the potential to remove approximately 80% of SO_4^{2-} from the aqueous solution at temperatures between 25 and 35 °C. The decline in SO_4^{2-} removal efficiency at higher temperatures can be attributed to changes in the adsorption process and sulphate release from the adsorbent itself, which was originally derived from sulphate-rich acid mine drainage (AMD). As temperature increases, the kinetic energy of SO_4^{2-} ions rises, potentially weakening electrostatic interactions and reducing their binding affinity to adsorption sites. Furthermore, SO_4^{2-} trapped within Al-rich Fe(III) species during adsorbent synthesis may undergo thermal desorption, leading to its release back into the solution, sometimes resulting in negative removal values.

Additionally, competitive adsorption from $H_2PO_4^-$ ions further limits the availability of active binding sites for SO_4^{2-}, displacing it from the adsorbent surface. This effect is exacerbated by the declining solubility of SO_4^{2-} at elevated temperatures, in accordance with Le Chatelier's principle, which predicts that higher temperatures reduce SO_4^{2-} retention on solid surfaces. Consequently, at temperatures above 35 °C, less SO_4^{2-} remains adsorbed, while increased desorption from the adsorbent matrix leads to a rise in the SO_4^{2-} concentration in the solution. These findings underscore the influence of the adsorbent's initial sulphate content on SO_4^{2-} behaviour under varying temperature conditions, highlighting the need for adsorbent optimisation to mitigate sulphate leaching in high-temperature applications [37,38].

For NO_3^- removal, an efficiency of ≥99% was observed at 25 °C, while PO_4^{3-} was almost completely removed (≥99.99%) at 35 °C. NH_4^+ was also fully removed at 25 °C. Therefore, 35 °C was identified as the optimum temperature for the removal of NH_4^+, PO_4^{3-}, and NO_3^- from the aqueous system.

3.1.4. Effect of pH

Figure 1d illustrates the attenuation of contaminants from synthetic municipal wastewater as a function of contact time, demonstrating exceptional stability in the removal of NO_3^-, NH_4^+, and PO_4^{3-}, with removal efficiencies exceeding 95% across the entire pH range. This high adsorption performance aligns with previous studies that have explored similar adsorbent materials for nutrient removal. Ma et al. [39] demonstrated that a ferric sulphate-modified carbon/zeolite composite effectively removed NH_4^+ and PO_4^{3-}, achieving high adsorption capacities across varying pH conditions due to the strong binding affinity of iron-based functional groups for these ions. Similarly, Cheng et al. [34] reported that Fe-Al bimetal composites efficiently removed NO_3^- from wastewater, maintaining stable performance despite fluctuations in solution chemistry, which is consistent with the findings in this study. The polycationic metals demonstrated effective SO_4^{2-} removal from the aqueous solution, particularly within the pH range of 5–8. At a lower pH, the adsorbent surface is positively charged, enhancing Coulombic attraction with negatively charged SO_4^{2-} ions. However, as the pH increases, surface deprotonation reduces the positive charge density, weakening electrostatic attraction and lowering sulphate adsorption efficiency. Additionally, $H_2PO_4^-$ acts as a competing anion, preferentially binding to active adsorption sites and displacing weakly held SO_4^{2-} ions. Since SO_4^{2-} has little competitive

influence on $H_2PO_4^-$, its removal efficiency continues to decline as pH increases. A similar trend was observed by Yamba et al. [40], who reported that sulphate removal efficiency decreases with increasing pH, further supporting the observed behaviour in this study. Overall, a pH of 7–8 was determined as the optimum range for the combined removal of SO_4^{2-}, NH_4^+, PO_4^{3-} and NO_3^-.

3.1.5. Treatment of an Authentic MWW Stream at Optimised Conditions

The attenuation of contaminants from authentic MWW under optimised conditions is summarised in Table 1.

Table 1. Attenuation results of contaminants from authentic MWW under optimised conditions.

Parameters	World Health Organization (WHO)	South African National Standards (SANS) 241	C_o (mg/L)	C_e (mg/L)	% Removal
PO_4^{3-}	No specific guideline	No specific standard for drinking water	420.8	<0.5	99.9
NH_4^+	≤1.5 mg/L	≤1.5 mg/L	180.7	<0.5	99.7
NO_3^-	≤50 mg/L	≤11 mg/L	226.0	2.114	99
SO_4^{2-}	≤250 mg/L	≤250 mg/L	253.9	9.138	96

As depicted in Table 1, the raw wastewater contained significant concentrations of oxyanions and ammonia, all of which exceeded the thresholds established by the World Health Organization (WHO) [41] and the South African National Standards (SANS) for drinking water. These elevated concentrations pose a significant environmental risk, as they promote the excessive growth of aquatic plants and complicate water treatment. However, after treatment with polycationic metals, the contaminants were efficiently removed, with the sequence of removal efficacy being $PO_4^{3-} \geq NH_4^+ \geq NO_3^- \geq SO_4^{2-}$.

PO_4^{3-} and NH_4^+ were particularly easy to remove, achieving near-complete removal rates. NO_3^-, while effectively removed, faced some challenges, likely due to the limited capacity of the polycationic metals or their specific reactivity with NO_3^-, which may require complementary treatment processes, such as reverse osmosis, for more complete removal [42]. Additionally, the presence of multiple competing ions in the wastewater could reduce the availability of reactive sites on the polycationic metals, further impacting NO_3^- removal efficiency [43,44].

A study by Ordonez et al. [45] utilised iron fillings to remove nutrients from wastewater, achieving removal efficiencies of 42% for NO_3^- and 98% for PO_4^{3-}. Similarly, Ma et al. [39] reported removal rates of up to 88% for NH_4^+ and 99% for PO_4^{3-} when using a ferric sulphate-modified carbon/zeolite composite. In terms of SO_4^{2-} removal, Nurmesniemi et al. [36] demonstrated that calcium sulphoaluminate can remove 98% of SO_4^{2-} from synthetic wastewater and 87% from industrial wastewater. Additionally, Xie et al. [46] investigated the removal of PO_4^{3-} from wastewater using calcium–aluminium layered double oxides with aluminium sludge, achieving a 98.85% removal rate. Overall, the use of polycationic metals recovered from real acid mine drainage in this study proved to be highly effective in removing contaminants from authentic MWW.

3.2. Characterisation Results of Sludge Samples

3.2.1. Functional Groups

Fourier Transform Infrared Spectroscopy (FTIR) was employed to characterise the functional groups of the recovered and valorised polycationic metals before and after their interaction with fortified authentic MWW [47]. Specifically, Figure 2 presents the functional groups identified in the polycationic metals following the removal of contaminants from

the aqueous media. This analysis provides insights into the chemical changes and bonding interactions that occurred during the adsorption process.

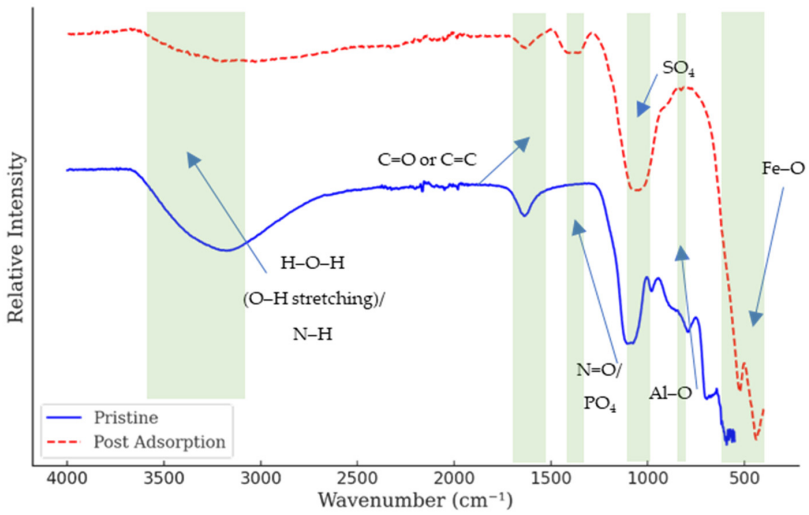

Figure 2. The FTIR spectra of pristine (blue) and post-adsorption (red dashed) samples illustrate structural and functional group modifications following contaminant adsorption. Notable changes include broad absorption peaks around 3500–3200 cm^{-1} (O–H and N–H stretching vibrations), 1700–1600 cm^{-1} (C=O and C=C functional groups), 1200–400 cm^{-1} (PO_4^{3-}, SO_4^{2-}), and circa 500 cm^{-1} (Fe–O). The green shaded regions highlight key wavenumber ranges affected by adsorption, further demonstrating modifications in the material's surface chemistry.

A summary of the peaks and bands corresponding to the different functional groups depicted in Figure 2 is provided in Table 2 to support and substantiate the results. This table highlights the key wavenumbers and their associated functional groups, offering a detailed understanding of the chemical interactions involved during the removal of contaminants.

As shown in Figure 2 and summarised in Table 2, the FTIR analysis reveals the peaks and bands associated with various functional groups in the polycationic metals after their reaction with SO_4^{2-}, NH_4^+, PO_4^{3-}, and NO_3^-. The results indicate Fe–O bending and stretching peaks between 438 and 528 cm^{-1} [48], signifying the presence of iron-based minerals. The Al–O peak signifies the involvement of aluminium-based minerals, indicating that aluminium oxides or hydroxides play a significant role in the formation of complexes with contaminants like phosphates and sulphates [49]. The Al–O bond is critical for binding phosphate ions, as aluminium exhibits a strong affinity for phosphate. The SO_4 stretching peak at 1082 cm^{-1} [50] suggests the formation of aluminium sulphate or oxyhydrosulphates.

Table 2. Functional groups and their respective wavenumbers and references.

Wavenumber (cm^{-1})	Functional Group	Reference
438–528	Fe–O	[48]
911	Al–O	[49]
1082	–SO_4	[51]
1425	N=O	[52]
1061–1645	–PO_4	[53]
3367	H–O–H	[54]
3404–3678	O–H stretching	[55]
3200–3500	N–H	[56]

The N=O peak suggests the presence of nitrate (NO_3^-) in the adsorbed state. Nitrates are likely bound to the surface of the polycationic metals through electrostatic interactions or coordination bonds with iron or aluminium [52]. The broad range of peaks corresponds to phosphate (PO_4^{3-}) groups, suggesting that phosphates are strongly bound to the surface of the polycationic metals, likely through the formation of aluminium or iron phosphate complexes [53]. The affinity of aluminium and iron for phosphate enhances the removal efficiency of PO_4^{3-} from wastewater [57].

The H–O–H bending peak indicates the presence of water molecules, suggesting that the polycationic metals are hydrated and that water plays a role in the adsorption process [54]. The hydration of the adsorbent is common in aqueous environments and can influence the adsorption capacity. The detection of hydroxyl (–OH) groups confirm that the sludge produced during the reaction is hydrated [55]. The presence of hydroxyl groups also implies that the metal oxides or hydroxides are in a hydrated state, which may enhance their reactivity and adsorption capacity.

The presence of the N–H group further demonstrates that the polycationic metals effectively removed NH_4^+ from the authentic MWW, as evidenced by its incorporation into the sludge [56].

Overall, the FTIR analysis provides strong evidence of the chemical interactions taking place between the polycationic metals and the various contaminants (SO_4^{2-}, NH_4^+, PO_4^{3-}, and NO_3^-). The identified functional groups confirm that iron and aluminium oxides or hydroxides are the primary active sites responsible for the adsorption of these contaminants. The presence of hydroxyl and water molecules further supports the notion that hydration plays a role in the overall adsorption process. The ability of these polycationic metals to adsorb multiple contaminants, including SO_4^{2-}, NH_4^+, PO_4^{3-}, and NO_3^-, highlights their versatility and effectiveness in wastewater treatment applications.

3.2.2. Elemental Properties

The elemental composition of the product sludge, following the removal of contaminants from authentic MWW, was analysed using Energy Dispersive X-Ray Spectroscopy (EDX), with the results presented in Figure 3.

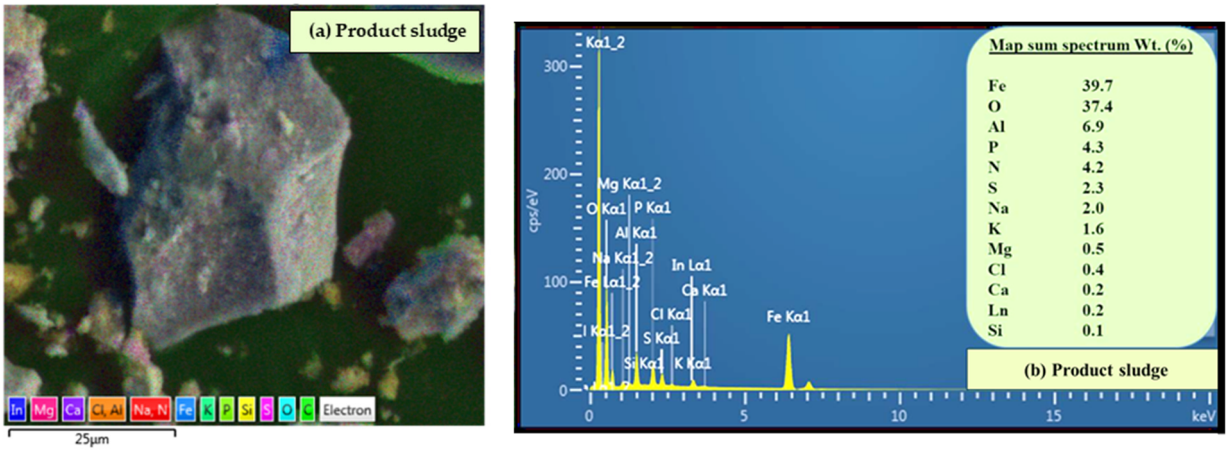

Figure 3. (**a**) SEM-EDS elemental mapping of the product sludge, highlighting the spatial distribution of key elements including Fe, O, Al, P, S, and other minor components. The false-colour mapping provides insight into the heterogeneous composition of the sludge, confirming the presence of adsorbed contaminants. (**b**) EDS spectrum of the product sludge, showing the relative elemental composition in weight percentages.

The EDX results confirm that iron (Fe), oxygen (O), and aluminium (Al) are the predominant elements in the polycationic metals, indicating the presence of Fe–O and Al–O

compounds. This finding aligns with the functional groups identified in the FTIR analysis, further supporting the involvement of iron and aluminium oxides in the adsorption process. Additionally, the presence of phosphorus (P), nitrogen (N), and sulphur (S) suggests that the contaminants, including SO_4^{2-}, NH_4^+, PO_4^{3-}, and NO_3^-, were successfully removed from the wastewater and incorporated into the sludge.

The detection of trace elements such as sodium (Na), potassium (K), magnesium (Mg), chlorine (Cl), calcium (Ca), lanthanides (Ln), silicon (Si), and carbon (C) provides further insights into the composition of the sludge. The presence of carbon is likely due to the sample coating used during the SEM measurements, rather than an inherent component of the sludge.

This comprehensive elemental analysis highlights the effectiveness of the polycationic metals in capturing and removing a wide range of contaminants from the authentic MWW matrix. The identification of key elements involved in the adsorption process validates the role of these metals in wastewater treatment and underscores their potential for targeting diverse chemical species.

3.2.3. Elemental Composition

The elemental composition of the product sludge after the removal of contaminants from authentic MWW was determined using X-Ray Fluorescence (XRF), with the results presented in Table 3.

Table 3. The elemental composition (wt.%) of the product sludge after the removal of contaminants from authentic MWW as measured by XRF.

Chemical Species	Composition (wt.%)	Chemical Species	Composition (wt.%)
Fe	46.82	Cl	1.14
P_2O_5	17.65	CaO	0.43
Al_2O_3	17.31	SiO_2	0.22
SO_3	4.02	BaO	0.06
Na_2O	3.53	Cs_2O	0.05
K_2O	3.29	Co_3O_4	0.04
MgO	1.30	Gd_2O_3	0.03
Chemical species	Composition (ppm)	Chemical species	Composition (ppm)
Mn	301	Yb	79
Zn	250	Bi	45
Pb	147	Cr	43
Ag	128		

As shown in Table 3, the product sludge's composition was dominated by iron (Fe) and aluminium (Al), which are key elements in AMD. The high concentrations of Fe (46.82 wt.%) and Al (17.31 wt.% in the form of Al_2O_3) reflect the polycationic metals' predominant role in the sludge. Phosphorus (P_2O_5, 17.65 wt.%) and sulphur (SO_3, 4.02 wt.%) were also abundant, confirming the effective removal of phosphate (PO_4^{3-}) and sulphate (SO_4^{2-}) from the wastewater.

Trace elements such as manganese (Mn), zinc (Zn), lead (Pb), silver (Ag), ytterbium (Yb), bismuth (Bi), and chromium (Cr) were present in smaller quantities. These elements were likely introduced from the AMD and retained in the sludge during the treatment process. On the other hand, the presence of sodium (Na_2O), potassium (K_2O), magnesium

(MgO), and calcium (CaO) in lower concentrations points to their association with the authentic MWW.

The XRF results align well with the findings from other analytical techniques, such as FTIR and SEM-EDX, confirming the effectiveness of the polycationic metals in capturing a wide range of contaminants from both AMD and authentic MWW. These results highlight the sludge's complex composition, reflecting both the original constituents of the AMD and the treated authentic MWW.

3.2.4. Morphological and Microstructural Properties

The morphological and microstructural properties of the product sludge were examined using Field Emission Scanning Electron Microscopy (FE-SEM). High-resolution images were captured, clearly revealing the fine microstructural details of the product sludge, as shown in Figure 4.

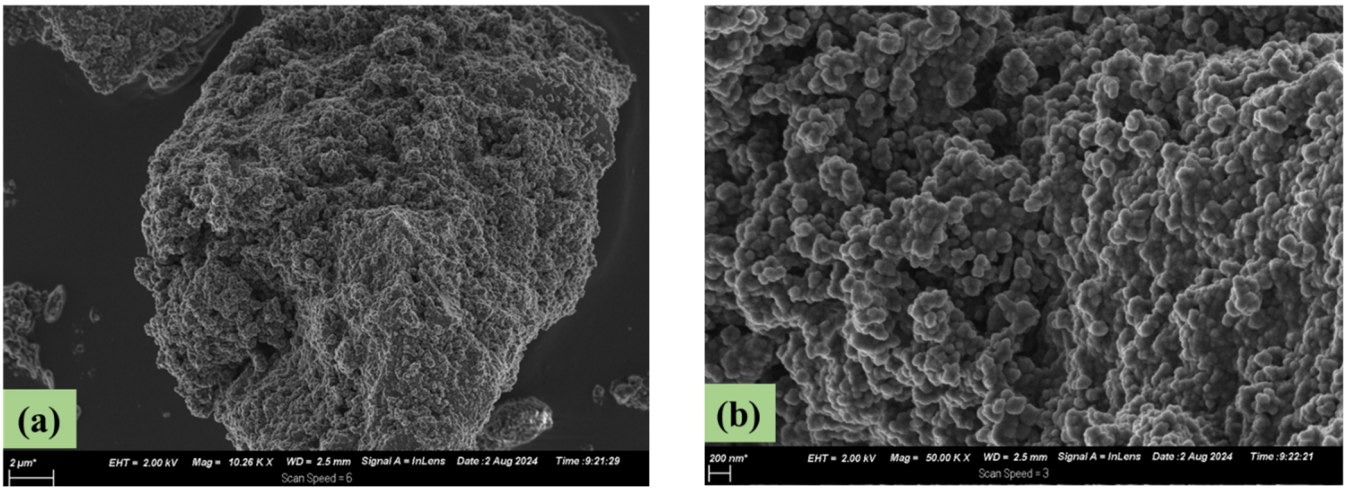

Figure 4. High-resolution FE-SEM microstructural images showing the morphological properties of the product sludge from the interaction of polycationic metals with contaminants in authentic MWW. (**a**) Low-magnification (10.26 kX) SEM image showing the overall morphology of the product sludge, revealing a rough and porous surface structure, which enhances its adsorption capabilities. (**b**) High-magnification (50 kX) SEM image illustrating the detailed surface texture, highlighting the presence of aggregated nanoscale structures and surface irregularities that provide active adsorption sites.

The product sludge exhibited a notable degree of homogeneity, with the surface predominantly consisting of spherical-like structures [58] interspersed with octagonal-like formations. These structures were uniformly distributed across the surface, indicating a consistent microstructural pattern throughout the sludge. A detailed examination across various magnifications, ranging from 2 µm to 200 nm, showed that the sludge retained its microstructural and morphological properties consistently. This uniformity across different scales confirms that the physical characteristics of the sludge do not vary significantly, suggesting structural stability [59].

Furthermore, the analysis confirmed that the product sludge exhibits a fully crystallised structure, with the SEM images revealing well-defined and uniform crystal lattices. This observation reinforces the conclusion that the minerals in the sludge are evenly distributed and crystallised [60]. The presence of these uniform crystal structures at all magnification levels supports the sludge's homogeneity and highlights its predominantly amorphous nature.

The SEM analysis underscores the stability and consistency of the sludge's composition and morphology, validating the efficiency of the treatment process in producing a uniform end product. The consistent microstructure and crystallinity suggest that the polycationic metals effectively facilitated the formation of a well-structured, stable sludge during the removal of contaminants from authentic MWW.

3.2.5. Elemental Mapping

In this section, the SEM micrograph and corresponding EDX elemental mapping of the product sludge are presented, as shown in Figure 5. The primary goal was to gain insights into the elemental composition of the product sludge after the removal of contaminants from authentic MWW [47]. The elemental mapping confirmed the presence of Fe, O, Al, P, S, N, Mg, and Ca, as depicted in Figure 5. These elements correspond to some of the peaks observed in the FE-SEM images, further substantiating the formation of polycationic metals. The rod-like structures primarily represent Fe, Al, and O, indicating the formation of polycationic metal complexes, while spherical structures suggest the presence of Mg, Ca, K, Mn, and Cl [47]. Overall, these results confirm the high efficacy of polycationic metals in removing contaminants from authentic MWW, with the adsorption process being particularly effective for capturing these elements from the aqueous matrix.

The chemical composition of the sludge, as revealed through the elemental analysis, suggests the formation of various compounds during the adsorption of contaminants. The following reactions illustrate the formation of different hydroxide compounds during the treatment process (Equations (5)–(8)).

Equation (5) illustrates the reaction between aluminium ions with hydroxide ions to denote the possible formation of aluminium hydroxide [61] from AMD.

$$Al^{3+} + 3OH^{-} \rightarrow Al(OH)_{3(s)} \quad (5)$$

Similarly, Equation (6) shows that iron ions combine with hydroxide ions to potentially form iron (III) hydroxide [62] from AMD.

$$Fe^{3+} + 3OH^{-} \rightarrow Fe(OH)_{3(s)} \quad (6)$$

In addition to the hydroxides, before the removal of contaminants from authentic MWW, the sludge contains magnesium and Ca, which can react with hydroxide ions to form potentially magnesium hydroxide, as illustrated in Equations (7) and (8).

$$Mg^{2+} + 2OH^{-} \rightarrow Mg(OH)_{2(s)} \quad (7)$$

$$Ca^{2+} + 2OH^{-} \rightarrow Ca(OH)_{2(s)} \quad (8)$$

Throughout the removal of contaminants from authentic MWW, the polycationic metals, predominantly composed of Fe and Al, adsorb ions such as NH_4^+, PO_4^{3-}, NO_3^-, and SO_4^{2-}. This process results in clean water that meets both World Health Organization (WHO) guidelines and South African National Standards (SANS 241) for various water uses. These reactions further demonstrate the efficiency of polycationic metals in removing a wide range of contaminants from wastewater while producing a stable, crystalline sludge.

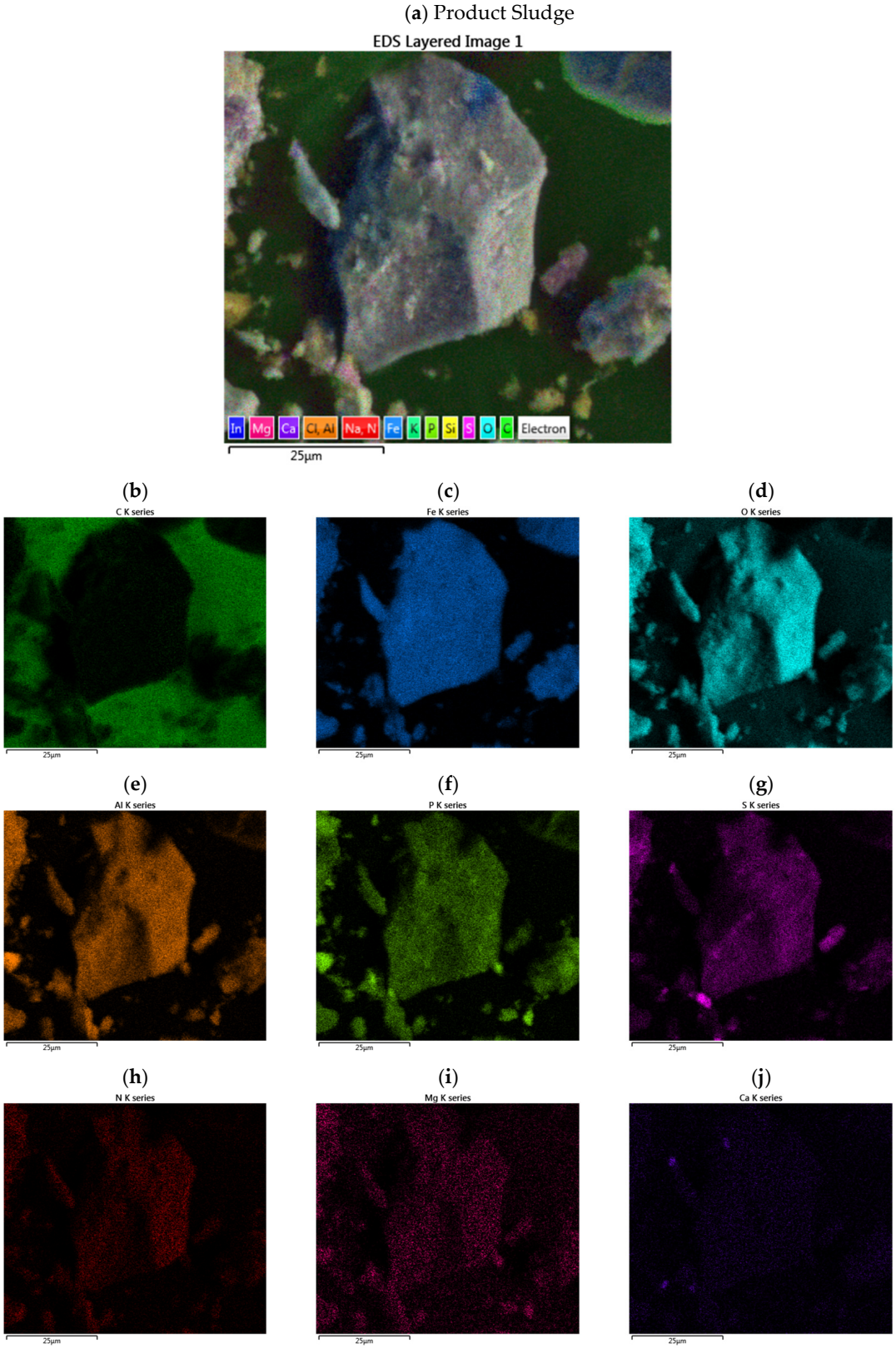

Figure 5. FE-SEM microstructural and elemental mapping of product sludge: (**a**) Field Emission Scanning Electron Microscopy (FE-SEM) image of the product sludge after contaminant removal from authentic municipal wastewater (MWW), showing its surface morphology. Elemental mapping using Energy Dispersive X-Ray Spectroscopy (EDX) confirms the distribution of key elements within the sludge: C (**b**), Fe (**c**), O (**d**), Al (**e**), P (**f**), S (**g**), N (**h**), Mg (**i**), and Ca (**j**). The presence of these elements indicates the successful adsorption of contaminants and validates the sludge composition following wastewater treatment.

3.3. Correlations Between Elements in SEM-EDX

Applying the method developed in Kpai et al. in 2023 [33], the elemental maps as presented in Figure 5 were correlated to establish the similarities between the elemental distributions in the maps. The resulting Pearson correlation coefficients are shown in Figure 6.

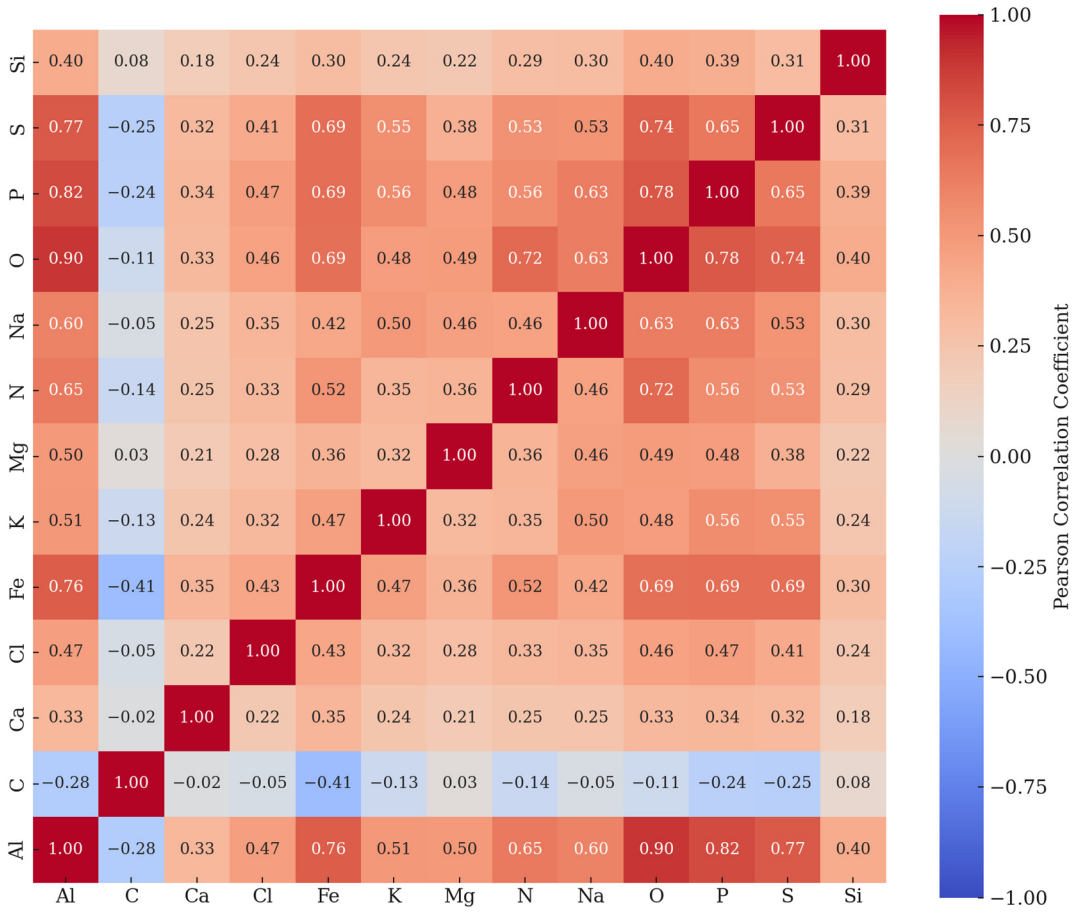

Figure 6. The heatmap presents the Pearson correlation coefficients between different elemental compositions in the product sludge, providing insights into their interrelationships. The colour gradient represents the strength and direction of correlations, with red shades indicating strong positive correlations (closer to 1.0), blue shades representing negative correlations (closer to −1.0), and white areas showing weak or no correlation (near 0.0).

The Pearson correlation coefficient matrix highlights several key relationships between the elements, reflecting their co-localisation and interaction in the material recovered from acid mine drainage (AMD) and utilisation for the adsorption of NH_4^+, PO_4^{3-}, NO_3^-, and SO_4^{2-}. Notably, the strong correlations involving phosphorus (P), nitrogen (N), sulphur (S), iron (Fe), and aluminium (Al) provide critical insights into the adsorption mechanisms.

3.3.1. Strong Correlations Involving P, N, and S

The correlations reveal that P and N are strongly associated with Fe and Al. P shows strong correlations with Fe (r = 0.69) and Al (r = 0.82), indicating that these elements form stable associations, likely as iron and aluminium phosphates. These phosphates are essential for the adsorption of PO_4^{3-} from wastewater, with iron and aluminium oxides acting as the primary adsorption sites [63].

Similarly, N, which may exist in the form of NH_4^+ or NO_3^-, also correlates strongly with Fe (r = 0.52) and Al (r = 0.65). This suggests that iron and aluminium oxides or hydrox-

ides serve as efficient adsorbents for nitrogen species, particularly NH_4^+. The material's ability to capture nitrogen compounds is closely tied to these strong elemental associations, with iron and aluminium compounds providing a reactive surface for adsorption through ion exchange or electrostatic interactions [45].

3.3.2. Role of Sulphur in Adsorption

S also demonstrates a strong correlation with Fe (r = 0.69) and Al (r = 0.77), indicating the presence of sulphur in the form of SO_4^{2-} or sulphide compounds. This strong association with iron and aluminium suggests that the material is well-suited for adsorbing sulphur-based contaminants, particularly SO_4^{2-} ions. Sulphur's strong correlation with iron likely reflects the formation of iron sulphides or the adsorption of SO_4^{2-} onto iron oxides, both of which are common in materials recovered from AMD [22].

The correlation between S and P (r = 0.65) further indicates the possibility of the co-adsorption of PO_4^{3-} and SO_4^{2-} ions in the same regions of the material. This could suggest the formation of mixed anionic adsorption sites on iron and aluminium oxides, where both SO_4^{2-} and PO_4^{3-} compete for surface binding, a behaviour observed in multi-anion adsorption systems [22].

3.3.3. Implications for Adsorption of NH4+, PO43−, NO3−, and SO42−

The strong correlations between P, N, S, Fe, and Al highlight the material's dual functionality, effectively adsorbing both cations (e.g., NH_4^+) and anions (e.g., PO_4^{3-} and SO_4^{2-}). Iron and aluminium oxides, formed during AMD treatment, serve as primary adsorption sites for both PO_4^{3-} and SO_4^{2-} ions, while their interaction with nitrogen species, particularly NH_4^+, enhances the material's overall adsorption capacity.

PO_4^{3-} and SO_4^{2-} are likely adsorbed through anion exchange processes, where they interact with the positively charged surface sites of iron and aluminium oxides [64].

NH_4^+ is adsorbed through ion exchange with the oxides, while NO_3^- may be removed through similar electrostatic interactions [65,66].

The coexistence of S and P with Fe and Al indicates that the material's surface is well-adapted to handling complex mixtures of contaminants, which are typical of wastewater streams that contain high levels of nitrogen, phosphorus, and sulphur compounds.

3.3.4. Moderate Correlations with Other Elements

While P, N, and S exhibit strong correlations with Fe and Al, moderate correlations were also observed with other elements. For example, magnesium (Mg) shows a moderate correlation with iron (Fe) (r = 0.36), suggesting that magnesium may also contribute to the structural stability of the material or act as a secondary adsorbent for certain ions.

3.3.5. Negative Correlations

A negative correlation was observed between Fe and Al with carbon (C) (r = −0.41 and r = −0.25, respectively), suggesting that C is likely present in a distinct phase, separate from the metal-based compounds. This carbon is likely a result of the sputtering process used to coat the material with carbon in preparation for SEM-EDX analysis. However, it appears that the carbon tends to "avoid" regions dominated by the metal phases, which is a point of interest.

The strong correlations between P, N, and S with Fe and Al underscore the material's effectiveness in adsorbing key contaminants such as PO_4^{3-}, NH_4^+, NO_3^-, and SO_4^{2-}. The interactions between these elements suggest that iron and aluminium oxides provide a highly reactive surface for the adsorption of both cations and anions, making the material versatile for treating wastewater streams with mixed contaminants. Sulphur's strong association with iron and aluminium further highlights the material's ability to capture

SO_4^{2-} ions, a common pollutant in acid mine drainage-affected waters. These findings emphasise the material's broad applicability in environmental remediation, particularly for the removal of nitrogen, phosphorus, and sulphur compounds from aqueous solutions.

3.4. Adsorption Kinetics

The transient data from the experimental runs were fitted using the pseudo-first-order and pseudo-second-order kinetics models (Equations (9) and (10), respectively [67]), and the kinetic data on the removal of contaminants from authentic MWW are shown in Figure 7 and summarised in Table 4.

$$\frac{dQ_t}{dt} = k_1(Q_e - Q_t) \quad (9)$$

$$\frac{dQ_t}{dt} = k_1(Q_e - Q_t)^2 \quad (10)$$

Table 4. Kinetics data on the removal of contaminants from aqueous solution.

Model/Model Parameters	NO_3^- (mg/L)	SO_4^{2-} (mg/L)	PO_4^{3-} (mg/L)	NH_4^+ (mg/L)
Pseudo first order				
Best-fit values				
Q_e	23.50	20.82	44.05	17.97
k_1	0.01864	0.02700	0.01800	0.3448
Goodness of Fit				
R squared	0.8718	0.9510	0.9548	0.9998
Sum of Squares	107.5	28.88	112.9	0.06530
Sy.x	3.919	2.031	4.017	0.09659
Pseudo second order				
Best-fit values				
k_1	0.0006240	0.001260	0.0003477	0.1436
Q_e	29.13	24.34	53.87	18.06
Goodness of Fit				
R squared	0.8407	0.9130	0.9332	0.9999
Sum of Squares	133.6	51.32	166.7	0.01568
Sy.x	4.369	2.708	4.881	0.04733

To assess the reliability and variability of the kinetic data, a 95% prediction interval was calculated for the adsorption kinetics model fits. The prediction interval provides an estimate of the range within which future observations are expected to fall with 95% confidence, accounting for both model uncertainty and inherent data variability.

For the pseudo-first-order and pseudo-second-order kinetic models (Equations (9) and (10)), the prediction interval was determined using the standard error of regression and the t-distribution [22].

In Figure 7, the 95% prediction intervals are shown as shaded regions around the model curves, representing the expected variation in contaminant removal efficiency. The narrow prediction intervals indicate a high degree of model reliability and strong agreement between experimental data and the fitted kinetic models.

By including this statistical analysis, the study ensures the robust interpretation of adsorption kinetics, improving the reliability of the findings for real-world wastewater treatment applications.

In analysing the adsorption kinetics for the removal of NO_3^-, SO_4^{2-}, PO_4^{3-}, and NH_4^+ from authentic MWW using polycationic metals, it is essential to determine the most suitable kinetic model that accurately reflects the adsorption behaviour of the system. Given the coexistence of multiple contaminants in the complex wastewater matrix, both

pseudo-first-order and pseudo-second-order kinetic models were exhaustively examined to identify the best fit.

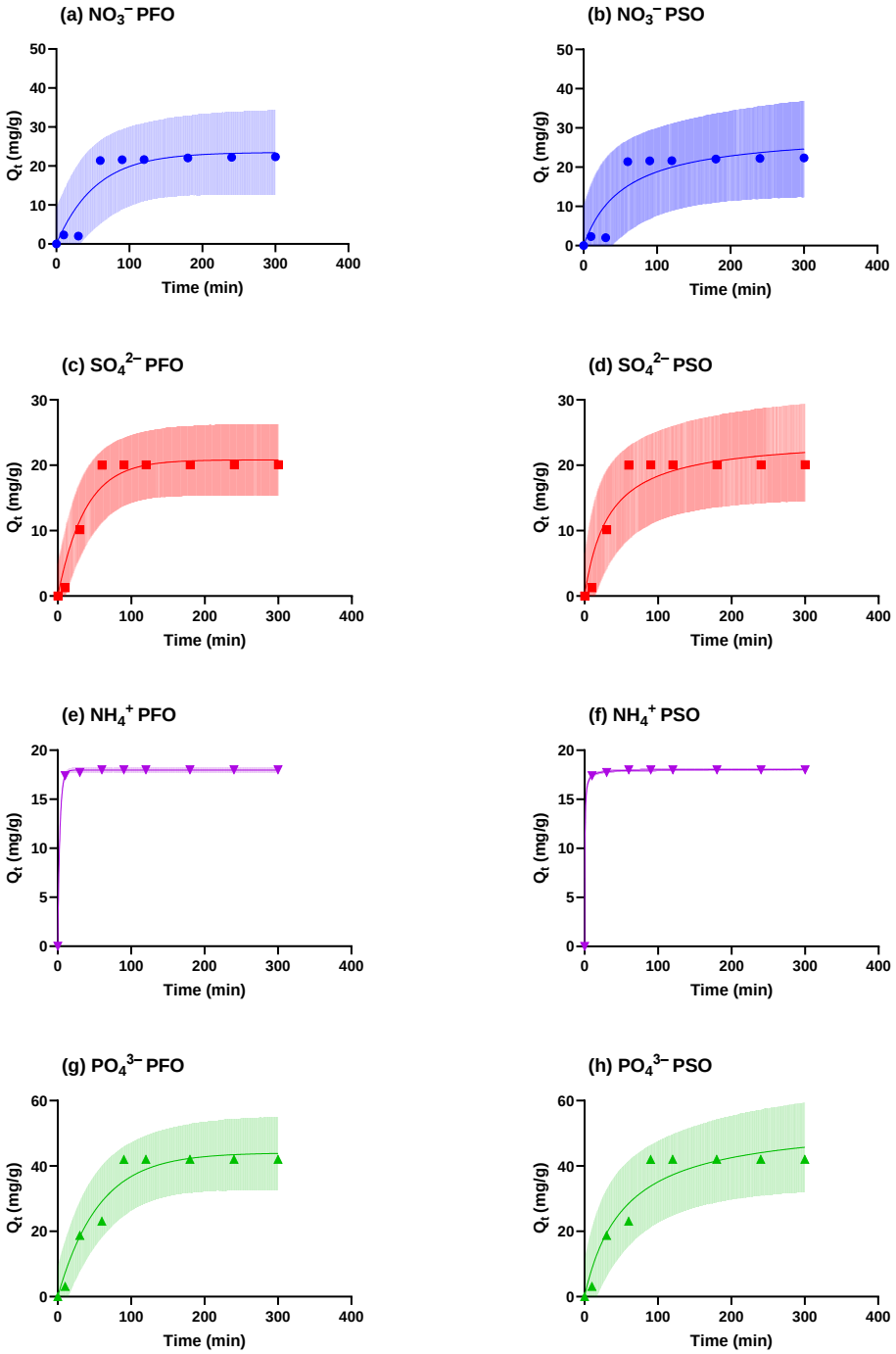

Figure 7. Kinetic model fits for the pseudo-first-order (PFO) (**a**,**c**,**e**,**g**) and pseudo-second-order (PSO) (**b**,**d**,**f**,**h**) adsorption models applied to the removal of NO_3^- (**a**,**b**), SO_4^{2-} (**c**,**d**), NH_4^+ (**e**,**f**), and PO_4^{3-} (**g**,**h**) from authentic municipal wastewater (MWW). Experimental data points are represented by markers, while solid lines indicate the model fits. The shaded regions represent 95% prediction intervals [22], showing the range within which future experimental values are expected to fall. These kinetic models provide insights into the adsorption mechanisms, highlighting differences in adsorption rates and equilibrium capacities for each contaminant.

The pseudo-first-order kinetic model exhibited strong correlations with the adsorption data, particularly for SO_4^{2-} (R^2 = 0.9510), PO_4^{3-} (R^2 = 0.9548), and NH_4^+ (R^2 = 0.9998), as shown in Table 4. These elevated R^2 values indicate a high degree of agreement between the

experimental data and the model predictions, especially for NH_4^+, where the fit was nearly perfect. For NO_3^-, however, the pseudo-first-order model displayed a slightly weaker fit (R^2 = 0.8718), suggesting that the adsorption mechanism for this contaminant may be more complex or influenced by additional factors not fully captured by the model. Despite this minor deviation, the pseudo-first-order model generally provides a robust representation of the adsorption kinetics for most contaminants.

On the other hand, the pseudo-second-order kinetic model performed exceptionally well for NH_4^+ (R^2 = 0.9999), indicating that the adsorption of ammonium ions is likely governed by chemisorption [22,67], characterised by stronger interactions between the adsorbate and the adsorbent. However, for contaminants like NO_3^- (R^2 = 0.8407) and SO_4^{2-} (R^2 = 0.9130), the pseudo-second-order model exhibited weaker correlations, implying that this model does not fully capture the adsorption kinetics for these species. The lower fit suggests that physisorption still plays a significant role [22,67], and the assumption of chemisorption may be less applicable to the adsorption of NO_3^- and SO_4^{2-}.

Considering the simultaneous presence of these contaminants in the same wastewater system, the overall adsorption kinetics align more closely with the pseudo-first-order model. The stronger and more consistent fit across key contaminants like SO_4^{2-}, PO_4^{3-}, and NH_4^+ supports this conclusion, particularly in scenarios where multiple ions are competing for adsorption sites. While the pseudo-second-order model performs significantly well for NH_4^+, its weaker fit for NO_3^- and SO_4^{2-} indicates that physisorption is the dominant mechanism driving the overall adsorption process. Consequently, the pseudo-first-order model emerges as the more appropriate representation of the adsorption kinetics for the removal of contaminants from authentic MWW using polycationic metals, suggesting that physical adsorption, with some influence of chemisorption for NH_4^+, largely characterises the process.

3.5. Adsorption Isotherms

The adsorption isotherms for the removal of contaminants from fortified authentic MWW using polycationic metals were examined to better understand the mechanisms governing the adsorption process. The Langmuir, Freundlich, and Two-Surface Langmuir isotherm models, shown in Equations (11)–(13), were applied to fit the equilibrium data [22,67].

$$Q_e = \frac{k_L Q_{max,L} C_e}{1 + k_L C_e} \tag{11}$$

This model assumes monolayer adsorption onto a surface with a finite number of identical sites.

- Q_e: amount of contaminant adsorbed per unit mass of adsorbent at equilibrium (mg/g);
- $Q_{max,L}$: maximum adsorption capacity (mg/g);
- k_L : Langmuir adsorption constant (L/mg), related to the affinity of binding sites;
- C_e: equilibrium concentration of the contaminant in solution (mg/L).

$$Q_e = K_F C_e^{\frac{1}{n}} \tag{12}$$

The Freundlich model describes multilayer adsorption on a heterogeneous surface.

- K_F: Freundlich constant, indicative of adsorption capacity;
- n: heterogeneity factor, indicating the favourability of adsorption;

$$Q_e = \sum_{i=1}^{2} \frac{k_{L,i}(T) Q_{max,i} C_e}{1 + k_{L,i}(T) C_e} \tag{13}$$

This model considers adsorption on two types of surfaces with different affinities and capacities.

- Q_e: amount of contaminant adsorbed per unit mass of adsorbent at equilibrium (mg/g);
- $Q_{max,i}$: maximum adsorption capacity of the i-th surface (mg/g);
- $k_{L,i}$: Langmuir constant for the i-th surface (L/mg);

These models provide insight into the nature of the adsorption process and help identify whether the adsorption is monolayer, multilayer, or occurs on multiple types of surfaces.

As depicted in Table 5 and Figure 8, the adsorption isotherm results offer insights into the adsorption behaviour of SO_4^{2-}, NH_4^+, PO_4^{3-} and NO_3^- using polycationic metals from fortified authentic MWW, elucidating the efficacy of different adsorption models.

Table 5. Adsorption isotherm models for removal of contaminants from fortified authentic MWW using polycationic metals.

Model/Model Parameters	NO_3^- (mg/L)	SO_4^{2-} (mg/L)	PO_4^{3-} (mg/L)	NH_4^+ (mg/L)
Langmuir				
Best-fit values				
Q_{MAX}	249.6	26.62	142.6	120.0
K_L	0.0073	0.06083	0.0714	0.003672
Goodness of Fit				
R squared	0.9842	0.9988	0.8844	0.9379
Sum of Squares	170.3	0.3875	1486	121.6
$S_{y \cdot x}$	4.932	0.3594	14.57	6.367
Freundlich				
Best-fit values				
K	3.459	6.436	24.52	1.435
n	1.346	3.675	2.576	1.486
Goodness of Fit				
R squared	0.971	0.991	0.9629	0.9511
Sum of Squares	311.7	3.012	476.8	95.84
$S_{y \cdot x}$	6.673	1.002	8.253	5.652
Two-Surface Langmuir				
Q_{MAX1}	0	0	13.58	3.61
Q_{MAX2}	249.6	26.62	169.3	170.8
K_{L2}	0.0073	0.06083	0.03042	0.001959
Goodness of Fit				
R squared	0.9842	0.9988	0.9416	0.9426
Sum of Squares	170.3	0.3875	750.8	112.4
$S_{y \cdot x}$	5.327	0.4402	11.19	7.498

For the contaminants under investigation, the Langmuir isotherm model demonstrates a robust fit for NO_3^- (R^2 = 0.9842), SO_4^{2-} (R^2 = 0.9988), and PO_4^{3-} (R^2 = 0.9379), signifying strong correlations in adsorption. Conversely, the fit for NH_4^+ is less robust (R^2 = 0.8844), indicating that the Langmuir model may not adequately encapsulate the adsorption characteristics of NH_4^+. The elevated Q_{MAX} values for NO_3^- (249.6 mg/g) and NH_4^+ (142.6 mg/g) denote a high adsorption capacity for these ions, while SO_4^{2-} and PO_4^{3-} exhibit moderate capacities of 26.62 mg/g and 120.0 mg/g, respectively. Despite the strong fit for most contaminants, the diminished correlation for NH_4^+ implies that the Langmuir model may not represent the most appropriate framework for elucidating the overall adsorption process within this system.

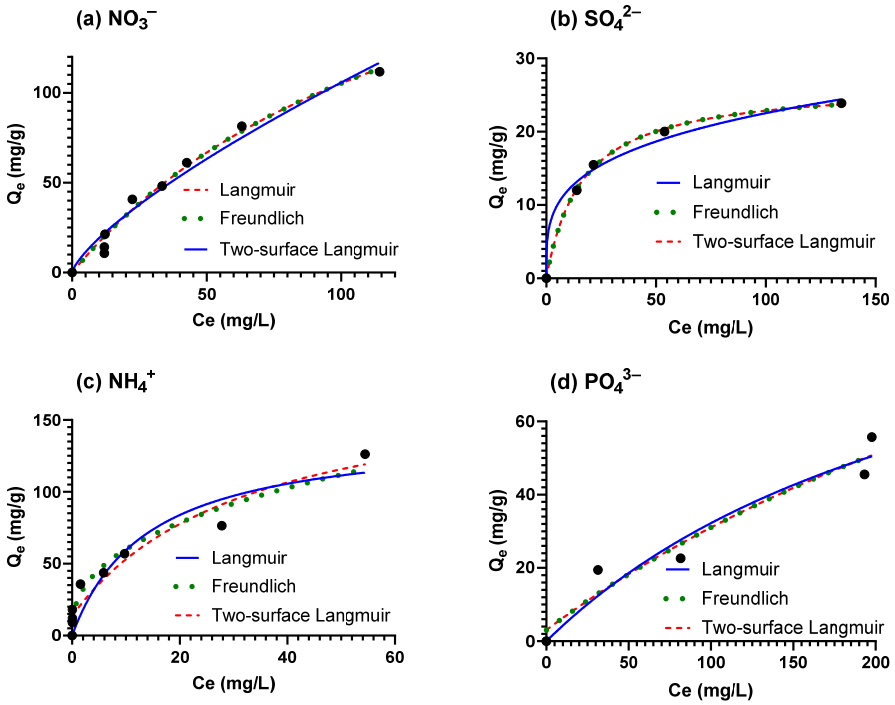

Figure 8. Adsorption isotherms illustrating the removal of NO_3^- (**a**), SO_4^{2-} (**b**), NH_4^+ (**c**), and PO_4^{3-} (**d**) from the aqueous system using polycationic metals. The experimental data points (black markers) are fitted to the Langmuir (solid line), Freundlich (dotted line), and Two-Surface Langmuir (dashed line) models, providing insight into the adsorption behaviour and mechanisms for each contaminant.

Similarly, the Freundlich isotherm model yields a reasonably good fit for all contaminants, with R^2 values of 0.971 for NO_3^-, 0.991 for SO_4^{2-}, 0.9629 for NH_4^+, and 0.9511 for PO_4^{3-}. This observation suggests that the Freundlich model can accommodate variations in adsorption energies across disparate sites. The parameter *n*, indicative of the intensity of adsorption, exceeds 1 for all contaminants (ranging from 1.346 for NO_3^- to 3.675 for SO_4^{2-}), thereby affirming favourable adsorption conditions. Although the Freundlich model does not yield the highest R^2 values in comparison to the Langmuir isotherm, it performs satisfactorily across all contaminants, indicating that adsorption may not exclusively transpire on a homogeneous surface and that multilayer adsorption may be influential, particularly for NH_4^+ and PO_4^{3-}.

Furthermore, the Two-Surface Langmuir isotherm model exhibits high performance for SO_4^{2-} (R^2 = 0.9988) and demonstrates strong correlations for NO_3^- (R^2 = 0.9842), NH_4^+ (R^2 = 0.9416), and PO_4^{3-} (R^2 = 0.9426). Additionally, this model indicates an elevated Q_{MAX2} for NH_4^+ (169.3 mg/g) and PO_4^{3-} (170.8 mg/g), signifying a superior adsorption capacity for these ions in contrast to the traditional Langmuir model. The enhanced fitting for NH_4^+ implies that this isotherm more accurately encompasses the intricate nature of the adsorption mechanism for NH_4^+, which may be affected by the existence of multiple adsorption sites. The Two-Surface Langmuir model, through its capacity to consider various types of adsorption sites, facilitates a more thorough comprehension of the adsorption dynamics of all contaminants, particularly within systems where adsorption may exhibit non-uniform characteristics.

Considering that the contaminants coexist within the same authentic MWW matrix, the Two-Surface Langmuir isotherm emerges as the most appropriate model for elucidating the overall adsorption dynamics. It provides exemplary fits for SO_4^{2-} and robust correlations for NO_3^-, NH_4^+, and PO_4^{3-}, while also accommodating the presence of multiple adsorption sites, which is likely in a complex wastewater environment. The increased adsorption

capacities (Q_{MAX2} values) for NH_4^+ and PO_4^{3-} further substantiate its relevance. Although the Langmuir and Freundlich isotherms yield insights into specific facets of the adsorption behaviour, the Two-Surface Langmuir model presents a more integrative representation of the adsorption phenomena concerning contaminants from authentic MWW utilising polycationic metals.

3.6. Proposed Adsorption Mechanism

The adsorption of contaminants such as SO_4^{2-}, NH_4^+, PO_4^{3-}, and NO_3^- from authentic MWW using polycationic metals recovered from acid mine drainage (AMD) operates through a combination of electrostatic interactions, ion exchange, and surface complexation mechanisms. The positively charged surfaces of the polycationic metals, primarily Fe and Al, attract negatively charged anions like SO_4^{2-} and PO_4^{3-} through electrostatic attraction. These anions then form surface complexes with the Fe and Al hydroxides present on the adsorbent's surface [22].

For cationic species such as NH_4^+, the removal occurs primarily through ion exchange mechanisms. The strong evidence for this mechanism comes from the rapid and nearly complete removal of NH_4^+ at a relatively low dosage of 1 g, indicating a strong affinity for NH_4^+. This removal occurs through the displacement of other cations (such as H^+) on the surface of the iron and aluminium oxides present in the polycationic metals. Furthermore, the adsorption of NH_4^+ follows pseudo-second-order kinetics, a characteristic behaviour of chemisorption, including ion exchange. This suggests that the interaction between NH_4^+ and the adsorbent is governed by a chemical process rather than mere physical adsorption, further supporting the ion exchange mechanism [45].

The presence of iron and aluminium oxides, which are known for their ion exchange capabilities, also provides structural evidence. The functional groups associated with these oxides, particularly hydroxides (–OH), act as exchange sites where NH_4^+ can displace other ions. Elemental analysis, such as the detection of nitrogen (N) in the post-adsorption material, supports the conclusion that NH_4^+ is successfully adsorbed onto the polycationic metals, reinforcing the role of ion exchange in the removal process [44].

In systems with multiple ions, such as PO_4^{3-}, NO_3^-, and SO_4^{2-}, competition for available adsorption sites occurs. PO_4^{3-} ions, due to their strong electrostatic interactions with Fe and Al hydroxides, have a higher affinity for the adsorption sites, resulting in superior removal efficiency compared to NO_3^-. The kinetic analysis suggests that the adsorption process follows pseudo-first-order kinetics for most contaminants, especially SO_4^{2-} and PO_4^{3-}, indicating that physical adsorption plays a significant role. However, the pseudo-second-order kinetics observed for NH_4^+ confirm that ion exchange dominates its removal [45].

Adsorption isotherms reveal that the Langmuir model fits the data well for NO_3^- and PO_4^{3-}, indicating monolayer adsorption on homogeneous sites. For NH_4^+, the Freundlich model suggests multilayer adsorption, pointing to a more heterogeneous process, likely due to the presence of multiple sites for ion exchange or chemisorption. Temperature also plays a key role in adsorption efficiency. As temperature increases, the removal of SO_4^{2-} decreases, consistent with the exothermic nature of the process. Conversely, higher temperatures enhance the adsorption of PO_4^{3-} and NH_4^+, likely due to increased diffusion rates or the overcoming of activation energy barriers.

In systems with multiple contaminants, co-adsorption and competition between PO_4^{3-} and SO_4^{2-} occur, as both are attracted to the same Fe and Al surface sites. This competition can reduce adsorption efficiency, particularly at higher temperatures or varying dosages. Ultimately, the polycationic metals demonstrate their versatility and effectiveness as adsorbents, capable of removing a wide range of contaminants from wastewater through both

physical adsorption and chemical bonding mechanisms, with ion exchange playing a key role in the removal of NH_4^+.

4. Conclusions and Recommendations

This study successfully demonstrated the recovery of polycationic metals (Fe^{3+} and Al^{3+}) from acid mine drainage (AMD) and their subsequent valorisation for municipal wastewater (MWW) treatment. The process effectively removed NH_4^+, SO_4^{2-}, PO_4^{3-}, and NO_3^- ions, achieving final water quality that meets WHO and South African National Water Standards under optimal conditions of 2 g of polycationic metals, 90 min of contact time, and a temperature of 35 °C.

The removal of contaminants was driven by a combination of ion exchange, surface complexation, and co-precipitation mechanisms, with pseudo-first-order kinetics indicating physisorption as the dominant process. Isotherm analysis best fit the Two-Surface Langmuir model, suggesting a mix of homogeneous and heterogeneous adsorption due to varying ion affinities for adsorption sites. Sludge characterisation confirmed the presence of Fe, Al, P, S, N, Mg, and Ca, further validating the adsorbent's ability to capture multiple contaminants through chemisorptive and electrostatic interactions.

Despite the clear potential of the recovered adsorbent, several challenges must be addressed to ensure large-scale applicability. These include scalability, competition from coexisting ions in complex wastewater matrices, long-term adsorbent stability, and regeneration efficiency. Understanding the mechanistic interactions between the polycationic metals and various contaminants will be crucial for optimising performance and improving adsorption selectivity. The further refinement of operational parameters, such as dosage control, contact time, and pH adjustments, will be necessary to enhance efficiency across different wastewater conditions.

Future research will focus on pilot-scale validation and industrial-scale implementation, ensuring that the system remains efficient, cost-effective, and adaptable to real-world treatment settings. Additionally, assessing the reusability and regeneration potential of the adsorbent will be critical in evaluating its economic and environmental feasibility. A comprehensive technoeconomic assessment will provide insights into the financial viability of the technology, while a life cycle assessment (LCA) will quantify its environmental impact and sustainability over time.

To further enhance contaminant removal efficiency and broaden applicability, hybrid treatment approaches combining adsorption with advanced oxidation processes, membrane-based separation, or biological treatments may be explored. These integrated strategies could improve pollutant removal while addressing challenges such as ion competition and adsorbent exhaustion, making the system more resilient and effective in diverse wastewater treatment applications.

Author Contributions: Conceptualisation, K.L.M., V.M. and H.G.B.; methodology, K.L.M., V.M. and H.G.B.; software, K.L.M., V.M. and H.G.B.; validation, V.M., H.G.B. and J.T.T.; formal analysis, K.L.M., V.M. and H.G.B.; investigation, K.L.M.; resources, V.M., H.G.B. and N.H.H.; data curation, K.L.M., V.M. and H.G.B.; writing—original draft preparation, K.L.M., N.H.H. and J.T.T.; writing—review and editing, V.M., H.G.B., N.H.H. and J.T.T.; visualisation, K.L.M., V.M. and H.G.B.; supervision, V.M. and H.G.B.; project administration, K.L.M., V.M. and H.G.B.; funding acquisition, K.L.M., N.H.H. and H.G.B. All authors have read and agreed to the published version of the manuscript.

Funding: This research was funded by the South Africa's National Research Foundation (NRF), Postgraduate Scholarship Grant ID No: MND200517522430. This work was further supported by the Austrian Federal Ministry of Education, Science and Research (BMBWF) through Austria's Agency for Education and Internationalization (OeAD) [Grant numbers: Africa UNINET P056 and P058 as well as APPEAR Project 341]. APPEAR is a program of the Austrian Development Organization.

Institutional Review Board Statement: Not applicable.

Informed Consent Statement: Not applicable.

Data Availability Statement: The raw data supporting the conclusions of this article will be made available by the authors upon request.

Acknowledgments: The authors would like to thank the University of Pretoria, the University of South Africa, and the Council for Scientific and Industrial Research for supporting this project. Furthermore, the staff from the municipal wastewater treatment house and mining houses are duly acknowledged for their support with sampling and access to the corresponding facilities. We would also like to thank the technicians in the corresponding laboratories who assisted with the analysis and characterisation of samples.

Conflicts of Interest: The authors declare no conflicts of interest. The funders had no role in the design of the study; in the collection, analyses, or interpretation of data; in the writing of the manuscript; or in the decision to publish the results.

References

1. Lin, L.; Yang, H.; Xu, X. Effects of Water Pollution on Human Health and Disease Heterogeneity: A Review. *Front. Environ. Sci.* **2022**, *10*, 880246. [CrossRef]
2. Xu, M.; Wang, Z.; Duan, X.; Pan, B. Effects of pollution on aquatic ecology and water quality bio-assessment. *Hydrobiologia* **2014**, *729*, 1. [CrossRef]
3. Price, J.I.; Heberling, M.T. The Effects of Source Water Quality on Drinking Water Treatment Costs: A Review and Synthesis of Empirical Literature. *Ecol. Econ.* **2018**, *151*, 195–209. [CrossRef] [PubMed]
4. Ahmed, S.; Kumar, P.; Kabir, M.; Zuhara, F.; Mehjabin, A.; Tasannum, N.; Hoang, A.; Kabir, Z.; Mofijur, M. Threats, challenges and sustainable conservation strategies for freshwater biodiversity. *Environ. Res.* **2022**, *214*, 113808. [CrossRef]
5. Rodriguez, M.; Rodriguez, M.; Baena-Moreno, F.; Vázquez, S.; Arroyo, F.; Vilches, L.; Zhang, Z. Remediation of acid mine drainage. *Environ. Chem. Lett.* **2019**, *17*, 137089.
6. Yuan, J.; Ding, Z.; Bi, Y.; Li, J.; Wen, S.; Bai, S. Resource Utilization of Acid Mine Drainage (AMD): A Review. *Water* **2022**, *14*, 2385. [CrossRef]
7. Shingwenyana, R.; Shabalala, A.N.; Mbhele, R.; Masindi, V. Techno-Economic Analysis of the Reclamation of Drinking Water and Valuable Minerals from Acid Mine Drainage. *Minerals* **2021**, *11*, 1352. [CrossRef]
8. Motsi, T.; Rowson, N.; Simmons, M. Adsorption of heavy metals from acid mine drainage by natural zeolite. *Int. J. Miner. Process.* **2009**, *92*, 42–48. [CrossRef]
9. Agboola, O. The role of membrane technology in acid mine water treatment: A review. *Korean J. Chem. Eng.* **2019**, *36*, 1389–1400. [CrossRef]
10. Dlamini, C.L.; De Kock, L.A.; Kefeni, K.K.; Mamba, B.B.; Msagati, T.A.M. Polymeric ion exchanger supported ferric oxide nanoparticles as adsorbents for toxic metal ions from aqueous solutions and acid mine drainage. *J. Environ. Health. Sci. Eng.* **2019**, *17*, 719–730. [CrossRef]
11. Anekwe, I.M.S.; Isa, Y.M. Bioremediation of acid mine drainage—Review. *Alex. Eng. J.* **2023**, *65*, 1047–1075. [CrossRef]
12. Le, V.-G.; Vu, C.-T.; Huang, Y.-H.; Shih, Y.-J.; Hien, V.; Nguyen, B.-S. Recovery of iron(II) and aluminum(III) from acid mine drainage by sequential selective precipitation and fluidized bed homogeneous crystallization (FBHC). *J. Taiwan Inst. Chem. Eng.* **2020**, *115*, 135–143. [CrossRef]
13. Masindi, V.; Foteinis, S.; Renforth, P.; Ndiritu, J.; Maree, J.P.; Tekere, M.; Chatzisymeon, E. Challenges and avenues for acid mine drainage treatment, beneficiation, and valorisation in circular economy: A review. *Ecol. Eng.* **2022**, *183*, 106740. [CrossRef]
14. Nur, T.; Johir, M.; Loganathan, P.; Nguyen, T.; Vigneswaran, S.; Kandasamy, J. Phosphate removal from water using an iron oxide impregnated strong base anion exchange resin. *J. Ind. Eng. Chem.* **2014**, *20*, 1301–1307. [CrossRef]
15. Kefeni, K.; Msagati, T.A.M.; Mamba, B. Acid mine drainage: Prevention, treatment options, and resource recovery: A review. *J. Clean. Prod.* **2017**, *151*, 475–493. [CrossRef]
16. Oyewo, O.; Agboola, O.; Onyango, M.; Popoola, P.; Bopape, M. Chapter 6—Current Methods for the Remediation of Acid Mine Drainage Including Continuous Removal of Metals from Wastewater and Mine Dump. In *Bio-Geotechnologies or Mine Site Rehabilitation*; Prasad, M.N.V., Favas, P.J.C., Maiti, S.K., Eds.; Elsevier: Amsterdam, The Netherlands, 2018; pp. 103–114.
17. Akinwekomi, V.; Maree, J.P.; Masindi, V.; Zvinowanda, C.; Osman, M.S.; Foteinis, S.; Mpenyana-Monyatsi, L.; Chatzisymeon, E. Beneficiation of acid mine drainage (AMD): A viable option for the synthesis of goethite, hematite, magnetite, and gypsum—Gearing towards a circular economy concept. *Miner. Eng.* **2020**, *148*, 106204. [CrossRef]

18. Akinwekomi, V.; Maree, J.P.; Zvinowanda, C.; Masindi, V. Synthesis of magnetite from iron-rich mine water using sodium carbonate. *J. Environ. Chem. Eng.* **2017**, *5*, 2699–2707. [CrossRef]
19. Aslam, T.; Masindi, V.; Ahmad, A.A.; Chatzisymeon, E. Valorization of Acid Mine Drainage into an Iron Catalyst to Initiate the Solar Photo-Fenton Treatment of Municipal Wastewater. *Environments* **2023**, *10*, 132. [CrossRef]
20. Wei, X.; Viadero, R.; Buzby, K. Recovery of Iron and Aluminum from Acid Mine Drainage by Selective Precipitation. *Environ. Eng. Sci.* **2005**, *22*, 745–755. [CrossRef]
21. Masindi, V.; Ndiritu, J.G.; Maree, J.P. Fractional and step-wise recovery of chemical species from acid mine drainage using calcined cryptocrystalline magnesite nano-sheets: An experimental and geochemical modelling approach. *J. Environ. Chem. Eng.* **2018**, *6*, 1634–1650. [CrossRef]
22. Muedi, K.L.; Brink, H.G.; Masindi, V.; Maree, J.P. Effective removal of arsenate from wastewater using aluminium enriched ferric oxide-hydroxide recovered from authentic acid mine drainage. *J. Hazard. Mater.* **2021**, *414*, 125491. [CrossRef]
23. Muedi, K.L.; Masindi, V.; Maree, J.P.; Brink, H.G. Rapid Removal of Cr(VI) from Aqueous Solution Using Polycationic/Di-Metallic Adsorbent Synthesized Using Fe3+/Al3+ Recovered from Real Acid Mine Drainage. *Minerals* **2022**, *12*, 1318. [CrossRef]
24. Muedi, K.L.; Masindi, V.; Maree, J.P.; Haneklaus, N.; Brink, H.G. Effective Adsorption of Congo Red from Aqueous Solution Using Fe/Al Di-Metal Nanostructured Composite Synthesised from Fe(III) and Al(III) Recovered from Real Acid Mine Drainage. *Nanomaterials* **2022**, *12*, 776. [CrossRef] [PubMed]
25. Agarwal, S.; Darbar, S.; Saha, S. Chapter 25—Challenges in management of domestic wastewater for sustainable development. In *Current Directions in Water Scarcity Research*; Elsevier: Amsterdam, The Netherlands, 2022; pp. 531–552.
26. Shetty, S.S.; Deepthi, D.; Harshitha, S.; Sonkusare, S.; Naik, P.B.; Kumari, N.S.; Madhyastha, H. Environmental pollutants and their effects on human health. *Heliyon* **2023**, *9*, e19496. [CrossRef]
27. Akinnawo, S.O. Eutrophication: Causes, consequences, physical, chemical and biological techniques for mitigation strategies. *Environ. Chall.* **2023**, *12*, 100733. [CrossRef]
28. Singh, B.J.; Chakraborty, A.; Sehgal, R. A systematic review of industrial wastewater management: Evaluating challenges and enablers. *J. Environ. Manag.* **2023**, *348*, 119230. [CrossRef]
29. Chen, Y.-n.; Liu, C.-h.; Nie, J.-x.; Luo, X.-p.; Wang, D.-s. Chemical precipitation and biosorption treating landfill leachate to remove ammonium-nitrogen. *Clean Technol. Environ. Policy* **2013**, *15*, 395–399. [CrossRef]
30. Bi, W.; Li, Y.; Hu, Y. Recovery of phosphorus and nitrogen from alkaline hydrolysis supernatant of excess sludge by magnesium ammonium phosphate. *Bioresour. Technol.* **2014**, *166*, 1–8. [CrossRef]
31. Zhou, Y.; Zhu, Y.; Zhu, J.; Li, C.; Chen, G. A Comprehensive Review on Wastewater Nitrogen Removal and Its Recovery Processes. *Int. J. Environ. Res. Public Health* **2023**, *20*, 3429. [CrossRef]
32. Muloiwa, M.; Dinka, M.; Nyende-Byakika, S. Application of Artificial Neural Network for predicting biomass growth during domestic wastewater treatment through a biological process. *Eng. Life Sci.* **2023**, *23*, e2200058. [CrossRef]
33. Kpai, P.Y.; Nel, J.; Haneklaus, N.; Chirwa, E.M.N.; Brink, H.G. Comparative Screening Study on the Adsorption of Aqueous Pb(II) Using Different Metabolically Inhibited Bacterial Cultures from Industry. *Water* **2023**, *15*, 4259. [CrossRef]
34. Cheng, H.; Zhu, Q.; Wang, A.; Weng, M.; Xing, Z. Composite of chitosan and bentonite cladding Fe-Al bimetal: Effective removal of nitrate and by-products from wastewater. *Environ. Res.* **2020**, *184*, 109336. [CrossRef] [PubMed]
35. Xu, H.; Wei, S.; Li, G.; Guo, B. Advanced removal of phosphorus from urban sewage using chemical precipitation by Fe-Al composite coagulants. *Sci. Rep.* **2024**, *14*, 4918. [CrossRef] [PubMed]
36. Nurmesniemi, E.-T.; Huhta, M.; Derkani, M.; Isteri, V.; Hanein, T.; Hu, T.; Tanskanen, P.; Lassi, U. Removal of sulphate and arsenic from wastewater using calcium sulfoaluminate (ye'elimite). *Front. Mater.* **2022**, *9*, 943486. [CrossRef]
37. Xu, N.; Christodoulatos, C.; Braida, W. Modeling the competitive effect of phosphate, sulfate, silicate, and tungstate anions on the adsorption of molybdate onto goethite. *Chemosphere* **2006**, *64*, 1325–1333. [CrossRef]
38. Chabok, Y.A.; Chourani, A. Adsorption of Sulfate in Aqueous Solutions by Cheap Plant Adsorbents. *Biosci. Biotechnol. Res. Asia* **2018**, *15*, 157–162. [CrossRef]
39. Ma, X.; Li, Y.; Xu, D.; Tian, H.; Yang, H. Simultaneous adsorption of ammonia and phosphate using ferric sulfate modified carbon/zeolite composite from coal gasification slag. *J. Environ. Manag.* **2022**, *305*, 114404. [CrossRef]
40. Yamba, S.; Hintsho-Mbita, N.C.; Yusuf, T.L.; Moutloali, R.; Mabuba, N. Sulphate Removal in Industrial Effluents Using Electrocoagulation Sludge as an Adsorbent. *Sustainability* **2022**, *14*, 12467. [CrossRef]
41. WHO. *Guidelines for Drinking-Water Quality*; WHO: Geneva, Switzerland, 2017; p. 631.
42. Schoeman, J.J.; Steyn, A. Nitrate removal with reverse osmosis in a rural area in South Africa. *Desalination* **2003**, *155*, 15–26. [CrossRef]
43. Bhatnagar, A.; Sillanpää, M. A review of emerging adsorbents for nitrate removal from water. *Chem. Eng. J.* **2011**, *168*, 493–504. [CrossRef]
44. Jadaa, W. Wastewater Treatment Utilizing Industrial Waste Fly Ash as a Low-Cost Adsorbent for Heavy Metal Removal: Literature Review. *Clean Technol.* **2024**, *6*, 221–279. [CrossRef]

45. Ordonez, D.; Valencia, A.; Chang, N.-B.; Wanielista, M.P. Synergistic effects of aluminum/iron oxides and clay minerals on nutrient removal and recovery in water filtration media. *J. Clean. Prod.* **2020**, *275*, 122728. [CrossRef]
46. Xie, N.; Yi, L.; Li, J.; Wang, W.; Gu, T.; Ma, M.-G.; Wang, S.; Liu, S. A green synthesis strategy toward calcined calcium-aluminum layered double hydroxide with sludge as aluminum source for efficient removal of phosphate from water. *Surf. Interfaces* **2024**, *46*, 104075. [CrossRef]
47. Wang, J.; Kong, F.; Liu, B.; Zhuo, S.; Ren, N.; Ren, H. Photogenerated carrier-accelerated 3D mesh-NH2 functionalized Zr-metal organic framework/MgAl-type hydrotalcite composites attacking diclofenac. *Sep. Purif. Technol.* **2025**, *354*, 128839. [CrossRef]
48. Ansari, M.S.; Raees, K.; Ali Khan, M.; Rafiquee, M.Z.A.; Otero, M. Kinetic Studies on the Catalytic Degradation of Rhodamine B by Hydrogen Peroxide: Effect of Surfactant Coated and Non-Coated Iron (III) Oxide Nanoparticles. *Polymers* **2020**, *12*, 2246. [CrossRef] [PubMed]
49. Romero, R.; Ruiz Santoyo, V.; Sánchez, C.; Rosales, M. Effect of aluminum precursor on physicochemical properties of Al2O3 by hydrolysis/precipitation method. *Nova Sci.* **2018**, *10*, 83. [CrossRef]
50. Tabelin, C.B.; Veerawattananun, S.; Ito, M.; Hiroyoshi, N.; Igarashi, T. Pyrite oxidation in the presence of hematite and alumina: I. Batch leaching experiments and kinetic modeling calculations. *Sci. Total Environ.* **2017**, *580*, 687–698. [CrossRef]
51. Mohamed, W.; Darweesh, S. Ancient Egyptian Black Patinated Copper Alloys. *Archaeom. J.* **2012**, *53*, 175–192. [CrossRef]
52. Osayemwenre, G.; Meyer, E.; Mamphweli, N. An outdoor investigation of the absorption degradation of single-junction amorphous silicon photovoltaic module due to localized heat/hot spot formation. *Pramana* **2015**, *86*, 901–909. [CrossRef]
53. Sun, D.-L.; Deng, J.-R.; Chao, Z.-S. Catalysis over zinc-incorporated berlinite (ZnAlPO4) of the methoxycarbonylation of 1,6-hexanediamine with dimethyl carbonate to form dimethylhexane-1,6-dicarbamate. *Chem. Cent. J.* **2007**, *1*, 27. [CrossRef]
54. Yusuf, M.O. Bond Characterization in Cementitious Material Binders Using Fourier-Transform Infrared Spectroscopy. *Appl. Sci.* **2023**, *13*, 3353. [CrossRef]
55. Kloprogge, J.T. Chapter 12—Infrared and Raman Spectroscopies of Pillared Clays. In *Developments in Clay Science*; Gates, W.P., Kloprogge, J.T., Madejová, J., Bergaya, F., Eds.; Elsevier: Amsterdam, The Netherlands, 2017; pp. 411–446.
56. Birsöz, B.; Baykal, A.; Toprak, M.; Koseoglu, Y. Synthesis, characterization and magnetic investigation of $(NH_4)0.5Mn1.25(H_2O)2[BP_2O_8]\cdot 0.5H_2O$. *Cent. Eur. J. Chem.* **2007**, *5*, 536–545. [CrossRef]
57. Pa Ho, H. Comparison of iron(III) and aluminum in precipitation of phosphate from solution. *Water Res.* **1976**, *10*, 903–907. [CrossRef]
58. Baghshahi, S.; Yousefi, F. A New Systematic Approach to the Morphology and Magnetic Properties of Spherical, Cubic, and Rod-like Magnetite Nanoparticles. *J. Supercond. Nov. Magn.* **2021**, *34*, 1949–1954. [CrossRef]
59. Liu, Y.; Chong, X.; Jiang, Y.; Zhou, R.; Feng, J. Mechanical properties and electronic structures of Fe-Al intermetallic. *Phys. B Condens. Matter* **2017**, *506*, 1–11. [CrossRef]
60. Zhang, X.; Wang, D.; Zhou, Y.; Chong, X.; Li, X.; Zhang, H.; Nagaumi, H. Exploring crystal structures, stability and mechanical properties of Fe, Mn-containing intermetallics in Al-Si Alloy by experiments and first-principles calculations. *J. Alloys Compd.* **2021**, *876*, 160022. [CrossRef]
61. Zhang, X.; Ye, P.; Wu, Y. Enhanced technology for sewage sludge advanced dewatering from an engineering practice perspective: A review. *J. Environ. Manag.* **2022**, *321*, 115938. [CrossRef]
62. Imai, R.; Kamimoto, Y.; Hagio, T.; Jung, Y.-J.; Ichino, R. Rapid determination of iron concentration in wastewater using color band formation. *SN Appl. Sci.* **2020**, *2*, 1517. [CrossRef]
63. Urano, K.; Tachikawa, H. Process-development for removal and recovery of phosphorus from waste-water by a new adsorbent.1. Preparation method and adsorption capability of a new adsorbent. *Ind. Eng. Chem. Res.* **1991**, *30*, 1893–1896. [CrossRef]
64. Acelas, N.; Mejia, S.; Mondragón, F.; Flórez, E. Density functional theory characterization of phosphate and sulfate adsorption on Fe-(hydr)oxide: Reactivity, pH effect, estimation of Gibbs free energies, and topological analysis of hydrogen bonds. *Comput. Theor. Chem.* **2013**, *1005*, 16–24. [CrossRef]
65. Ion, I.; Bogdan, D.; Mincu, M.; Ion, A. Modified Exfoliated Carbon Nanoplatelets as Sorbents for Ammonium from Natural Mineral Waters. *Molecules* **2021**, *26*, 3541. [CrossRef] [PubMed]
66. Palko, J.; Oyarzun, D.; Ha, B.; Stadermann, M.; Santiago, J. Nitrate removal from water using electrostatic regeneration of functionalized adsorbent. *Chem. Eng. J.* **2018**, *334*, 1289–1296. [CrossRef]
67. Largitte, L.; Pasquier, R. A review of the kinetics adsorption models and their application to the adsorption of lead by an activated carbon. *Chem. Eng. Res. Des.* **2016**, *109*, 495–504. [CrossRef] [PubMed]